Components of the Plasma Membrane of Growing Axons. III. Saxitoxin Binding to Sodium Channels

GARY R. STRICHARTZ, ROCHELLE K. SMALL, and KARL H. PFENNINGER
Department of Anesthesia Research Laboratories, Harvard Medical School, Boston, Massachusetts 02115; and Department of Anatomy and Cell Biology, Columbia University, College of Physicians and Surgeons, New York 10032. Dr. Small's present address is Department of Pathology (Immunology), Yale University School of Medicine, New Haven, Connecticut 06510.

ABSTRACT The density of sodium channels was measured in growing and mature axons of the olfactory nerve of the bullfrog, using as a probe the drug saxitoxin (STX). The toxin binds to control nerves from adult animals in a saturable manner with a dissociation constant of ~23 nM at 4°C and a capacity of 72 fmol/mg wet weight, equivalent to about five sites per square micrometer of axolemma. In growing nerves, obtained from adult frogs 4–5 wk following removal of the original nerve, the STX-binding capacity per wet weight of tissue is markedly reduced, to ~25% of control values, and appears to decrease in the proximodistal direction.

STX-binding data, expressed as STX/mg wet weight, was converted to STX/μm^2 of axolemma using stereologically derived values of membrane area per milligram wet weight of nerve. The axolemmal content (area/mg wet weight) of all regions of growing nerve is substantially decreased compared to controls, but increases in the proximodistal direction by 60%. These changes in axolemmal area result in calculated STX receptor densities (per unit axolemmal area) which, in distal regions, are approximately at the level of the mature nerve and, in proximal regions, are actually increased above cotrols by 50 to 70%.

Upon comparing the axolemmal density of intramembrane particles, reported in the companion paper, with the calculated density of STX receptors in both mature and growing nerves, we find a correlation between STX receptors and intramembrane particles with diameters of 11.5–14.0 nm. The growing axon's gradient of sodium channels and the shift from this gradient to a uniform distribution in the mature axon suggest (*a*) that sodium channels are inserted into the perikaryal plasmalemma and diffuse from there into the growing axolemma, and (*b*) that the axolemma undergoes functional maturation during growth.

During differentiation, neurons extend axonal and dendritic processes and become capable of producing regenerative action potentials (23, 37). Action potentials usually result from the inward flow of sodium ions across the nerve membrane through discrete sodium channels (15) whose probability of opening is transiently increased during membrane depolarization (16). These sodium-dependent action potentials are often not the first type of regenerative impulses to appear during development, but are preceded by calcium-dependent impulses (37) that have a different ion selectivity and pharmacology and are mediated by a transmembrane channel different from that generating sodium-dependent impulses (11). Eventually, however, the impulses in a mature axon are dependent exclusively on ionic currents passing through voltage-dependent sodium channels.

The drugs tetrodotoxin (TTX)[1] and saxitoxin (STX) are specific inhibitors of the sodium channel in most excitable membranes. Both toxins bind reversibly and with high affinity to channels in intact cells and membrane fragments, and to solubilized toxin receptors (for review, see reference 30). The measurement of uptake of radiolabeled toxins has been applied previously to assay the spatial distribution of sodium channels in nerve and muscle cells (3, 12, 31).

[1] *Abbreviations used in this paper:* e.c.s., extracellular space; STX, saxitoxin; TTX, tetrodotoxin; *STX, tritiated saxitoxin.

THE JOURNAL OF CELL BIOLOGY · VOLUME 98 APRIL 1984 1444-1452

The development of sodium channels has not been directly and quantitatively assayed previously in neurons in vivo. Electrophysiological experiments on neuroblastoma cells in culture have demonstrated the existence of sodium currents in axonal processes and cell bodies, (23) and ion flux studies indicate that these channels have a pharmacology like that of mature cells in vivo, particularly with respect to their sensitivity to TTX and STX (2, 38). Other studies on regenerating (18, 19) or remyelinating (34) mammalian axons have reported changes in excitability parameters or in STX-binding values that strongly suggest real changes in the membrane density of sodium channels.

In this paper, we describe studies on the binding of tritiated saxitoxin (*STX) to follow the appearance of sodium channels during growth and differentiation of nonmyelinated axons. A further goal was to correlate the spatial distribution of STX receptors with the distribution of intramembrane particles in growing and mature axolemma (see our companion papers, references 35, 36).

MATERIALS AND METHODS

Nerve Preparations: Adult bullfrogs (*Rana catesbeiana*) were maintained and subjected to surgery as described in one of our preceding companion papers (36); a segment from both of their olfactory nerves was removed to induce well synchronized, *de novo* growth of axons. Mature and growing nerves were removed for binding studies from animals (at least 400 g body weight) anesthetized with ~3 ml of 3% ethyl-m-amino benzoate injected into the ventral lymph sac. The skin was cut away from the nares to a point between the eyes, and bone and cartilage were removed to expose the olfactory nerve along its entire length. The nerve, accompanied by much of the olfactory bulb, was then dissected free. The tough perineurium was removed from the nerve under 25X magnification before the incubation phase of the binding experiments. The nerves were kept in a frog Ringer solution (see below) after their dissection from the animal and maintained at 0°C, except for the time during which the perineurium was removed.

The lengths of mature and growing unfixed nerves that had been soaked for varying periods were found to be considerably shorter than those of undissected nerves fixed in vivo. Therefore, the lengths of incubated nerve segments were normalized to the length of nerves fixed in vivo, using the average total length determined in the previous study (36). The identical procedure was applied to mature and growing axons.

Toxin Binding Experiments: Binding experiments were conducted at 4 or 10°C. For most experiments the whole nerves were incubated for 6 h to achieve the equilibrium state of STX-receptor binding. The nerves were then removed from the incubation vials and sectioned transversely along their length into several segments. In the cases of control tissues, nerves were also split longitudinally to provide two tissue samples of the same proximodistal segment. (The term "proximal" designates nerve segments close to the perikarya that are located peripherally in the nasal cavity, while "distal" designates segments closer to the terminals in the olfactory bulb [see Fig. 1].) During this division the lengths of the nerves and their segments were measured under a calibrated stereomicroscope and recorded. The pieces of nerve were then gently blotted on Whatman No. 1 filter paper (Whatman Laboratory Products Inc., Clifton, NJ) to remove any solution remaining on the surface and weighed on a torsion balance (Bethlehem Balance Co., Bethlehem, PA). Individual nerve pieces were sealed in glass scintillation vials containing 100 μl H_2O and 500 μl tissue solubilizer (Protosol, New England Nuclear [NEN], Boston, MA). After digestion for 8–12 h at room temperature (20–22°C), scintillant (5 ml Aquasol 2; NEN or Dimiscint, National Diagnostics, Somerville, NJ) was added to the vials and the radioactivity measured in a liquid scintillation counter. Samples of the soaking solution were also counted to confirm the value of the free *STX concentration. The addition of aliquots of calibrated tritiated water to some samples permitted the determination of counting efficiency.

STX uptake was measured as fmol/mg wet weight of nerve. Values are presented as means plus-or-minus standard errors. The total *STX uptake is the sum of the saturable binding component to sodium channels and a component that is linearly dependent upon toxin concentration (17). The linear *STX uptake was determined in the presence of excess (10^{-6} M) unlabeled TTX, a competitive inhibitor of STX binding (4, 14).

The data used in this paper include STX uptake measurements in segments from the intranasal (proximal) region and from the bone collar to the distal regions (cf. Fig. 1). Binding data from intranasal segments were included, even though electron microscopy showed that most growing neurites in this region were contained in very fine fascicles (diam < 10 μm) which were too small to be desheathed without major axonal damage and therefore were excluded from the incubated preparation. Examination of electron micrographs of the remaining large intranasal fascicles, which were included in the incubated preparations, revealed a relatively large volume of extra axonal space and, thus, a reduced axolemmal area per milligram wet weight of nerve. Therefore, calculation of *STX binding per unit membrane area in the included proximal segments are almost certainly underestimates of the true receptor density.

The kinetics of STX uptake by mature olfactory nerves were followed in two experiments at 10°C in 2.0 nm *STX. Toxin uptake increased progressively from the time of the first measurement, at 2 h, to 5–7 h, when it reached a constant value (in fmol/mg wet weight). By 8 h of incubation, however, STX uptake had begun to fall by ~10%. For this reason, all the equilibrium binding experiments reported in this paper were done by incubating nerves in *STX for periods of 5.5 to 6.5 h, and all nerve pieces in any one experiment were removed from the incubation solutions within a 45-min interval.

The total *STX uptake by growing nerves varied less in time than that of mature nerves. When the uptakes were compared during incubations lasting 6–9 h, in four separate experiments, the ratios of the total uptake (in fmol/mg wet nerve) at longer times (7–9 h) to the total uptake for the shortest incubations (6 h) were close to unity: for proximal segments, 1.04 ± 0.14; for bone collar regions, 0.98 ± 0.05; for middle segments, 1.01 ± 0.16. (There were too few samples to average data from distal segments of growing nerves.) These results demonstrate that the STX uptake of growing nerve was relatively stable over incubation periods of 6–9 h. Still, in most of the experiments we limited the incubation period of the nerves in STX to 6–7 h.

It is unclear why the STX-binding activity of mature nerves falls after 7 h at 4–10°C. In previously reported binding studies using bundles of small nonmyelinated fibers or membranes isolated from rabbit brain, the uptake of STX and TTX did not diminish during incubation for up to 8 h (4, 33, 39, 41). One possible explanation for the apparent loss of binding activity is an increase in wet weight of the olfactory nerves, perhaps due to slowing of the Na^+-K^+ pump in the cold and concomitant increases in intracellular Na^+ and water. This possibility was ruled out, however, by measurements of the extracellular space and of the protein per milligram wet weight of nerve (Bio-Rad protein assay, Bio-Rad Laboratories, Inc., Richmond, CA). Over an 8-h incubation, the inulin-accessible space of the distal half of the nerve changed by <14%, whereas the proximal half of the nerve showed a 27% loss of inulin-accessible space.

The protein content of nerve segments, also measured over an 8-h incubation period, varied by <6% in distal segments (mean value: 83.9 ± 12.7 μg protein/mg wet weight from a total of 20 measurements over this period), whereas the proximal halves apparently increased in protein content by ~30%, rising from 85 to 110 μg protein/mg wet weight of nerve (mean value: 101.2 ± 12.6 from 22 measurements). These results, taken together with the apparent reduction of inulin-space, suggest that the proximal nerve segments are actually losing water during incubation. In contrast to the proximal segment, the inulin-accessible space and protein/mg wet weight of the distal segment appear to be very stable during long incubations. Thus, the drop in binding activity per wet weight of nerve clearly is not caused by an increase in the wet weight of the tissue after long incubation, and its origin remains unknown.

*STX was prepared by the method of Ritchie et al. (33). The STX was exposed to 25 Ci of ^3H_2O by NEN for 3 h at 50°C. After removal of the ^3H_2O, the rapidly exchangeable tritium nuclei were washed out by water at 10°C. The resulting labeled STX was further purified by high-voltage paper electrophoresis and its concentration determined by a bioassay procedure (5). Paralytic shellfish poison (Food and Drug Administration, Cincinnati, OH) was used as the standard in this bioassay. The purity of the toxin was determined by the method of Levinson (25) and ranged from 76% to 89% for the three *STX preparations used. The true specific radioactivity of the toxin preparations ranged from 8.2 to 11.8 Ci/mmol.

The frog Ringer solution consisted of 110 mM NaCl, 2.0 mM $CaCl_2$, 2.5 mM KCl, 5 mM HEPES:NaOH, pH 7.2. A dry mixture of toxins containing STX was supplied by the Toxicology Study Section of the National Institutes of Health (Bethesda, MD). TTX and HEPES buffer were purchased from Calbiochem-Behring Corp. (La Jolla, CA). Ethyl-m-amino benzoate was purchased from Sigma Chemical Co. (St. Louis, MO). All other salts and chemicals were of reagent grade. Tritiated water, [^{14}C]mannitol, and [^{14}C]inulin were purchased from NEN.

Morphometric Analysis: Tissues were processed for electron microscopy as described earlier (36). Cross-sections of two segments along the proximodistal axis of mature nerves and three segments of growing (4–5 wk) olfactory nerves were quantitatively examined to determine the cellular volume fractions and surface density (area per unit volume) of axolemma.

For each segment of nerve, tissue from three to four frogs was sampled.

Thin sections were cut through the entire cross-sectional area of growing nerves and half the cross-sectional area of mature nerves. Sections were examined on a JEOL JEM 100C electron microscope, calibrated with a replica grating (E. F. Fullam, Schenectady, NY). Two sections from each tissue block were randomly photographed at × 16,000, using the corners of the grid spaces (150-mesh) as the criterion for selecting areas.

Analyses were carried out according to standard stereological procedures (e.g., reference 47; cf. reference 45), taking advantage of an Apple II Plus computer. Micrographs were printed at × 46,000 and analyzed with a test grid consisting of 10 rows, each containing six 2-cm test lines, whose endpoints described a square lattice. Point counting (endpoints of test lines) was used to determine the relative volumes of the following compartments of the nerve: axons, Schwann cells, other cell types, clusters or large, clear vesicles, and extracellular space (including basal lamina and collagen fibers). The volume of the vascular compartment was similarly calculated but on micrographs taken at lower magnification.

The frequency of intersections of plasma membranes with test lines determined the relative surface density of membranes of different cell types. Axonal surface density was calculated with the formula, $S_v = \pi I_L/2$ for cylinders cut in cross-section, where I_L is the density of axolemmal intersections per unit of test line.

To convert binding data expressed as *STX/mg wet weight to *STX/μm^2 of axolemma, we assumed a nerve buoyant density of 1.05 mg/mm^3. This appears to be a reasonable assumption on the basis of the densities known for intact cells (1) and those of most subcellular fractions of the nerve (9).

The number of axons contained in the nerve was determined by counting the number of axons per unit area of cross-sections and referring this relative number to the entire cross-sectional area of that nerve segment. An outline of a 1 μm thick section of the nerve segment was traced onto a Houston Instruments digitizing pad using a Leitz microscope drawing tube. The tracing followed the contour of the most peripheral axonal bundles thereby excluding the sheath and its underlying space. This data was relayed to an Apple II Plus computer equipped with a program for digitizing morphological parameters (R & M Biometrics, Knoxville, TN).

RESULTS

Stereological Results

The diagram of isolated olfactory nerves, shown in Fig. 1, indicates the average lengths of mature and growing nerves and the position of the morphological landmarks used in this study. The stereological data are derived from sections taken from the zones lettered A–C, which were each 0.5 mm wide. Toxin binding was measured in continuous segments that were 3.0 and 1.5–2.0 mm long in mature and growing nerve, respectively, and that were identified by their position along the nerve axis. To compare the stereological data with the toxin-binding values, we related the average of the morphometric values from the two bounding zones (e.g., A and B) to the binding capacity of the nerve segment spanning those zones (e.g., AB, the bone collar segment). Since the lengths of the nerve segments and the distance between sampling zones were shorter in growing than in mature nerves, both these parameters were referred to the initial narrowing of the bone collar at zone A as an origin.

STEREOLOGY OF MATURE NERVES: In the middle region of mature nerve $7.18 \cdot 10^6$ axons comprise 49% of the nerve volume, Schwann and other cell types occupy 17% of the volume, and the extracellular space (e.c.s.) some 34% of the volume (Tables I and II). The nerve becomes more compact along its proximodistal axis as it travels from segment A, the region of convergence of axon fascicles, to segment B in the middle region (cf. schematic of segments in Fig. 1). The e.c.s. compartment decreases from 38% to 31% of the nerve volume, thus increasing the cellular volume fractions and the density of plasma membranes. Axolemmal surface density increases by 10% from 8,250 mm^2/mm^3 to 9,200 mm^2/mm^3 between segments A and B. These values suggest a slightly larger axolemmal content than that found in the pike olfactory nerve by von Muralt et al. (45).

STEREOLOGY OF GROWING NERVES: At 4 to 5 wk postoperative, the growing nerve contains $1.36 \cdot 10^6$ axons, which comprise only ~10% of the nerve volume (Tables I and II). The e.c.s. is about twice that of mature nerves, and decreases from 62% of the nerve volume in segment A to 54% of the volume in segment B, where the axon fascicles have converged into a compact bundle. Axolemmal surface density almost doubles in this region, from 1,190 mm^2/mm^3 to 2,100 mm^2/mm^3, reflecting both an increased cellular density as the nerve becomes more compact and a greater

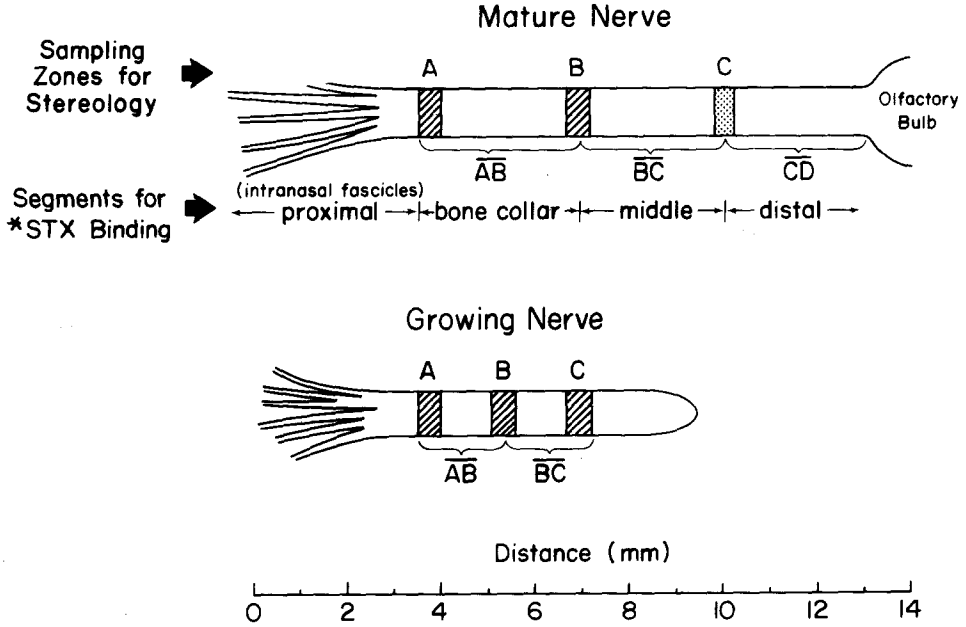

FIGURE 1 Scale diagram of nerves showng markers for morphological parameters (stereology) and *STX binding. *STX uptake was measured in segments corresponding, for example, to the region normally encased in a bone collar of the skull ($\overline{AB}$) and was related to the average of the axolemmal areas in the bounding zones (*A* and *B*). The dimensions shown are for those of a nerve fixed in situ.

TABLE I

Summary of Stereological Analysis of Mature Olfactory Nerves (Rana catesbeiana)

Mature	Nerve segment* A	AB	B
Axolemma, surface density (mm^2/mm^3)	8,250 ± 460 (3)‡	8,730	9,200 ± 190 (3)
Volume fractions			
Axons	0.446 ± 0.019 (3)	0.485	0.523 ± 0.013 (3)
Schwann	0.110 ± 0.022 (3)	0.118	0.125 ± 0.015 (3)
Other cell types	0.069 ± 0.005 (3)	0.056	0.042 ± 0.008 (3)
Extracellular space	0.377 ± 0.029 (3)	0.344	0.310 ± 0.020 (3)
No. axons in nerve		$7.18 \cdot 10^6 \pm 0.61$	

* Refer to Fig. 1 for comparison of corresponding nerve segments in growing and mature nerves. BC and CD are the average of two contiguous segments.
‡ All values are means ± SEM, number of data points in parentheses.

TABLE II

Summary of Stereological Analysis of Growing Olfactory Nerves (Rana catesbeiana)

Growing*	A	AB	B	BC	C
Axolemma, surface density (mm^2/mm^3)	1,190 ± 360 (3)	1,650	2,100 ± 350 (4)	2,000	1,900 ± 310 (3)
Volume fractions:					
Axons	0.070 ± 0.018 (3)	0.097	0.124 ± 0.023 (4)	0.119	0.113 ± 0.026 (3)
Schwann	0.166 ± 0.008 (3)	0.197	0.227 ± 0.032 (4)	0.196	0.165 ± 0.006 (3)
Other cell types	0.148 ± 0.013 (3)	0.127	0.106 ± 0.016 (4)	0.101	0.096 ± 0.018 (3)
Extracellular space	0.617 ± 0.036 (3)	0.580	0.543 ± 0.057 (4)	0.584	0.625 ± 0.029 (3)
No. axons in nerve			$1.36 \cdot 10^6 \pm 0.10$		

* 4–5 wk postoperative.

irregularity in axonal profiles, probably associated with the not too distant growth cones. Further towards the growing tip, in segment C, axolemmal surface density remains high at 1,900 mm^3/mm^3 while the other cellular compartments decrease; the e.c.s. increases to 63% of the nerve volume.

To determine if the morphology of the perfused nerves used for stereology was similar to that of nerves incubated in STX at low temperatures, we compared the stereologic e.c.s. data with the volume accessible to "extracellular" marker molecules in the nerves incubated in the cold for 6 h. Indeed, in mature nerves these two methods yielded nearly identical values after subtraction of the vascular compartment, which appears to be sealed off. The inulin-accessible space in the bone collar and middle segments (0.35 ± 0.02 and 0.29 ± 0.01 μl/mg wet wt, respectively) agreed closely with the morphologically determined e.c.s. in fixed tissue (0.38 ± 0.03 and 0.31 ± 0.02 μl/mg wet wt, respectively). The same comparison in growing nerves showed that the inulin-accessible space accounted for only ~75% of the extravascular interstitial space determined stereologically in both the bone collar region and middle segment. This discrepancy may reflect the much higher collagen content apparent in the e.s.c. of growing nerves.

STX Binding to Mature Nerves

As in other nerve preparations, total STX uptake is the sum of a saturable (U_{sat}) and a linear (U_{lin}) component:

$$U_{tot} = U_{sat} + U_{lin} = U_{max}\frac{[STX]}{[STX] + K_D} + b[STX],$$

where U_{max} is the total number of STX receptors, or the toxin-binding capacity of the tissue, and K_D is the equilibrium dissociation constant. The coefficient of linear uptake, b, is a characteristic parameter of a particular tissue preparation and is unrelated to saturable *STX binding. Thus, the calculated difference between the measured total STX uptake, U_{tot}, and U_{lin} is U_{sat}, which is a hyperbolic function of STX concentration. Fig. 2*A* shows linear and saturable *STX uptakes from a typical binding experiment. The parameters U_{max} and K_D may be derived from a Scatchard plot of the saturable binding data (Fig. 2*B*) where, for a single class of binding sites, U_{sat}/[STX] vs. U_{sat} gives a straight line graph. For the experiment of Fig. 2, the slope of this line, $-1/K_D$, results in a K_D = 17.1 nM, and the x-axis intercept, U_{max}, equals 66 fmol/mg wet wt. Parameters of *STX binding to mature nerves are summarized in Table III. From a total of six separate binding experiments of the type shown in Fig. 2, the average value for K_D equals 22.9 ± 3.4 nM. Average U_{max} values were determined from Scatchard plot analysis of saturation curves, as in Fig. 2*B*, plus U_{sat} measurements at single concentrations of *STX and the application of the hyperbolic binding equation, introduced above, using the average K_D values in Table III. For mature nerves, U_{max} equals 72.0 ± 5.9 fmol/mg wet wt.

The uptake of *STX was characterized in different segments along the axis of mature nerves. Fig. 3*A* shows the linear and saturable uptakes from one experiment at 4 nM *STX by various nerve segments from three bullfrogs. In other, similar experiments, mature nerves were bisected transversely, near the B zone (cf. Fig. 1), and *STX uptakes measured in the proximal and distal halves. The results of all such experiments are shown in Table III. Two aspects of STX binding are apparent: (*a*) Linear uptake (coefficient b) decreases gradually in the proximodistal direction by 24%. The linear uptake is the result of *STX distributed in the e.c.s. of the nerve and that bound by weak ionic association to the negatively charged axonal and glial membranes (32, 39). As concluded from the measurements of inulin space and the morphometric analysis (Tables I and II), the reduction of U_{lin} distally is probably

largely due to a decrease (18%) in extracellular space within the nerve. (*b*) No significant difference exists between saturable *STX-binding parameters in more proximal compared to more distal segments of nerve, the average values of K_D being 21.4 ± 7.1 (3) and 23.4 ± 3.4 nM (2), respectively, and those of U_{max} being 74.2 ± 5.0 (5) and 71.0 ± 7.0 (4) fmol/mg wet weight, respectively.

The saturable binding capacity (U_{max}) can be expressed as a surface density of receptors (Table III, fourth column) by application of the morphometric data listed in Tables I and II, and an assumed specific density for this nerve tissue of 1.05 gm/cm^3 (cf. Materials and Methods). The calculated *STX receptor densities of the more proximal and more distal segments of mature nerves are essentially the same, being 5.68/μm^2 and 4.88/μm^2, respectively. (If we treat the accumulated errors in the density calculation [Δ values in Table III] as the standard errors of the mean density measurement, and assume a normal distribution of data, then the calculated mean densities in proximal and distal halves do not differ significantly, judged by the two-tailed Student's *t* test: $0.25 < P < 0.40$.) Thus, the density of STX receptors appears to be uniform along the mature bullfrog nerve.

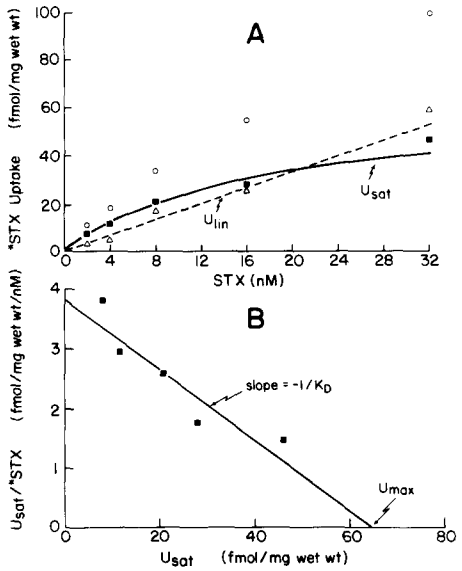

FIGURE 2 (*A*) Components of *STX uptake by proximal halves of mature nerves. Saturable binding (U_{sat}, ■) is the difference between total uptake (○) and the linear uptake calculated from measured uptakes (△) in the presence of unlabeled TTX (1 μM). The average linear uptake coefficient, *b*, which is the slope of the broken line in *A* (see text), was multiplied by the free [*STX] to determine a U_{lin} corresponding to each concentration of *STX for which total binding was measured. Each data point represents uptake by one piece of nerve that averaged 1.5–2 mg wet weight. (*B*) Scatchard plot of the saturable *STX binding resolved in *A*. The line is a least squares fit to the points (correlation coefficient = 0.925), and graphs the equation $U_{sat}/[*STX] = (U_{sat} - U_{max})/K_D$. For this experiment U_{max} = 65.9 fmol/mg wet weight and K_D = 17.1 nM.

Saxitoxin Binding to Growing Nerves

4–5 wk after surgery the saturable STX-binding activity of the growing nerves is substantially reduced (Table IV). The results of one typical experiment are shown in Fig. 3*B*. Linear uptake is measurably increased over controls in all segments, corresponding to the large increase noted in e.c.s. Saturable *STX binding per milligram wet weight is reduced in all segments of growing nerves compared to controls. Saturable and linear *STX uptakes by growing nerve were usually measured at only one concentration of *STX and compared to uptake by mature nerves measured at the same time, because of the paucity of tissue in growing nerves. Measurements of the relative saturable binding of *STX in all experiments on growing nerve are summarized in Table IV. When expressed on a wet weight basis the average saturable STX binding by all segments of growing nerves is ~25% of control

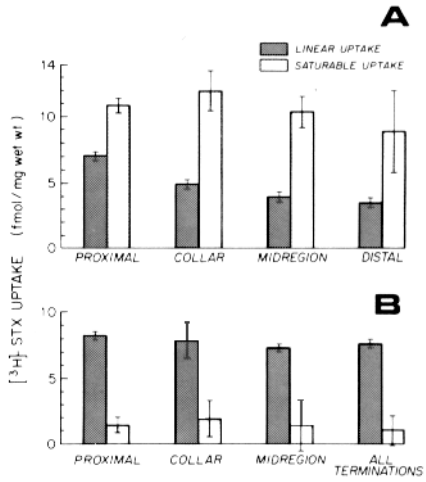

FIGURE 3 (*A*) Control nerve. (*B*) Growing nerve (4 wk postoperative). Uptake of *STX by segments of mature and growing nerves. Segments as diagrammed in Fig. 1. Growing nerves terminated in the collar ($\overline{AB}$) or the middle region ($\overline{BC}$), the average of *STX uptakes by all distal terminations is shown by the right-most bar of the lower panel. Uptakes were measured at 4 nM *STX and 10°C. Each value is the mean uptake by three nerve samples; error bars shown ± SEM.

TABLE III

Parameters of STX Binding by Mature Nerves*

Segment	K_D	U_{max}‡	*b* = linear uptake coeff.	Calculated density STX receptors§
	nM	*fmol/mg wet wt*	*fmol/mg wet wt/nM*	*μm^{-2}*
Proximal and collar	21.4 ± 7.1 (3)	74.2 ± 5.0 (5)	1.61 ± 0.16 (16)	5.680 (Δ 0.70)
Middle and distal	23.4 ± 3.4 (2)	71.0 ± 7.0 (4)	1.22 ± 0.16 (17)	4.88 (Δ 0.59)
All segments‖	22.9 ± 3.4 (6)	72.0 ± 5.9 (10)	1.40 ± 0.08 (37)	5.29 (Δ 0.63)

* Values are means ± SEM with number of data points in parentheses.
‡ The larger number of measurements of U_{max} than of K_D results from additional experiments using only single concentrations of STX (see Results).
§ Derived by application of the stereological data from Table I; areas per milligram wet weight of zone B were used to calculate the density of receptors in middle and distal segments, and the average of zones A and B (AB) to calculate the average density for all segments. Errors (Δ values) represent the sum of the percent errors (SEM per mean) of area plus U_{max} values.
‖ Includes data from whole nerves not sectioned into smaller segments.

TABLE IV

STX Receptor Density in Growing Nerve*

Nerve segment	Relative U_{sat}‡ (fraction of control)	Relative axolemmal area§ (fraction of control)	Receptor density relative to control¶	Absolute**
Proximal	0.246 ± 0.063 (Δ 3)	0.145 (Δ 0.051)‖	1.70 (Δ 1.04)‖	9.66 (Δ 5.59)/μm^2‖
Bone collar	0.282 ± 0.087 (Δ 3)	0.189 (Δ 0.058)‖	1.49 (Δ 0.74)‖	8.46 (Δ 3.97)/μm^2‖
Middle	0.286 ± 0.154 (Δ 2)	0.218 (Δ 0.117)‖	1.31 (Δ 0.97)‖	6.40 (Δ 4.74)/μm^2‖

* 4–5 wk postoperative.

‡ Measured at 4–16 nM, and compared to U_{sat} of control nerves, measured at the same time. Values are means ± SEM, number of separate experiments in parentheses.

§ Refer to zones diagrammed in Fig. 1. Proximal: A; collar: (A + B)/2; middle: (B + C)/2: absolute values from Table I.

‖ Δ numbers in parentheses are the sums of the percentage errors of the factors (whose product is the specified parameter), multiplied by the mean value of the parameter: e.g., relative axolemmal area = area A (growing)/area A (mature) = α. Thereby, (Δ) of relative axolemmal area = α [SE area A (growing)/area A (growing) + SE area A (mature)/area A (mature)].

¶ Relative U_{sat} divided by relative axolemmal area.

** Relative densities of growing nerve divided by respective densities of mature nerve. Proximal and bone collar segments: multiplied by average control densities for all proximal and collar segments of mature nerves (5.68/μm^2); for middle segments: multiplied by average densities of all distal and middle segments of mature nerves (4.88/μm^2).

values, from eight separate relative uptakes using 4–16 nM *STX. Relative U_{sat} at all measured *STX concentrations was about the same, suggesting that the K_D for STX binding was the same for receptors in growing and mature nerve and, consequently, that reductions in saturable binding were due to changes in U_{max}.

Among the various segments, the standard errors are large, ranging from 26% to 54% of the mean values. Most of this variation is attributable to the large variance in the measured values of U_{tot} in the small pieces of growing nerves; the combination of lowered specific binding (U_{sat} per milligram wet weight) and smaller tissue samples often resulted in *STX uptake by growing nerves being reduced to 10% or less than that of the equivalent mature nerve segment. Nevertheless, considering the large standard errors, the results are quite consistent.

A segmental analysis of the relative saturable STX uptake per milligram wet weight reveals no significant regional differences along the growing nerve (Table IV). However, the axonal membrane area per wet weight is also reduced in growing nerves, resulting from a major loss in the number of axons (cf. Tables I and II). Reductions of axolemmal area actually exceed those of STX binding sites, particularly in the more proximal nerve segments. As a result, the calculated density of STX receptors per membrane area in the more proximal segments of 4–5 wk growing nerves increases over that of control nerves (Table IV, third column). In the collar and middle regions of growing nerves the calculated receptor densities are elevated above control densities by 50% and 30%, respectively. This trend is continued in the intranasal proximal segments of the nerves, where uncertainties in wet weight per axon and in morphometric parameters are relatively large (cf. Materials and Methods); here the STX receptor density is increased by ~70% over controls. Since in these proximal nerve segments the axonal content per milligram wet weight is almost certainly lower than in more distal regions, the true increase in STX receptor density per axonal membrane area is probably even larger. The corresponding absolute densities of STX receptors per membrane area range from 6.4–9.7/μm^2 in growing nerves. Within the accumulated error, the calculated mean densities for STX receptors indicate a gradient of STX-binding sites in the proximodistal direction in growing nerves.

In two experiments the binding of *STX to nerve sheath and to the nonneural "stumps" at the distal ends of the growing nerve was measured. In neither case was the uptake affected by the presence of unlabeled TTX, revealing an absence of detectable high-affinity STX-binding sites. In the nerve "stumps," probably composed of glia and fibroblasts, the linear uptake was about equal to that of axon-containing segments. Thus, there is no evidence in our studies that such glia bind STX with high affinity.

DISCUSSION

Structural Considerations

The morphologies of growing and mature olfactory nerves differ markedly, as indicated by the changes in the relative volumes occupied by axons, other cell types, and the e.c.s. (Tables I and II). All regions of the growing nerve show a drastic reduction in axolemmal content. Moreover, the axolemmal surface density shifts regionally, decreasing to a lesser relative extent in the more distal portions of the growing nerve. This results in a proximodistal increase in the absolute axolemmal area reflecting both the greater heterogeneity of axonal profiles seen distally and the presence of larger numbers of highly irregular growth cones with a large surface: volume ratio. Therefore, a segmental analysis of axolemmal surface density is required for any calculation of the true membrane densities for STX receptors along the growing nerve.

STX Binding and Sodium Channels

In this paper we assume that all sodium channels in the bullfrog olfactory nerve axons are blocked by the low concentrations of STX used and therefore, that all sodium channels are accounted for by the class of STX receptors with K_D ~23 nM. This assumption is probably true for both mature and growing nerves. No reports exist of STX-resistant sodium channels in vertebrate nerves. Although there is evidence that vertebrate muscle cells express a TTX- or STX-resistant sodium channel under certain conditions, particularly early in development (13, 20, 40), the sodium channels displayed by vertebrate neurons in culture are all of the TTX-sensitive variety (2, 23, 38). In other STX-binding experiments, a combination of electrophysiological and biochemical data has shown that one STX molecule binds to one sodium channel (14, 42), and in the present experiment, the U_{max} values of bullfrog nerves also represent the tissue density of sodium channels. The relative amount of nonneural elements is quite large in the growing olfactory nerves, making the measure-

ment of U_{sat} more difficult ($U_{sat} \ll U_{lin}$). However, it has been shown that STX does not bind saturably to nonaxonal elements in amphibian nonmyelinated nerve (44) and our studies on nerve sheath and "stumps" bear this out. Therefore, we believe that the saturable component of STX binding can be identified exclusively with sodium channels in the axolemma of the olfactory nerve.

The STX receptor is described by two parameters, tissue site density (U_{max}) and equilibrium dissociation constant (K_D). These measures amount to 70–75 fmol/mg wet wt and ~23 nM (at 4–10°C), respectively, in mature olfactory nerves of the bullfrog. This is both a lower density and a slightly weaker affinity than has been reported previously for STX binding in other preparations of nonmyelinated fibers. In terms of tissue density, the toxin-binding capacities in axons of the rabbit vagus, lobster walking leg, and garfish olfactory nerves are 100 ± 7, 94 ± 5, and 377 ± 17 fmol/mg wet weight, respectively, which correspond to estimated site densities of 110, 90, and 35 per μm^2 of axonal membrane (33). The STX receptor density per unit area of membrane of bullfrog olfactory axons reported here is five per μm^2, a low value compared to the ones estimated for other nonmyelinated axons, including those of the olfactory nerve of the garfish. However, if the *STX-binding capacity is expressed with respect to the protein content of the mature nerves, using an average value from proximal and distal samples of 92.5 μg protein/mg wet weight (see Materials and Methods), then U_{max} is equivalent to ~0.8 pmol/mg protein of whole nerve, a value that is 40–80% of the binding capacities reported for enriched synaptosomal preparations from mammalian brain (17, 48). On this basis the U_{max} value of 72 fmol/mg wet wt is reasonably comparable to that expected for whole nerve preparations. This agreement supports the calculated density of 5 sites per μm^2. In addition, and of major importance is the fact that, unlike the other studies on neurons, our results are based on binding studies and stereology conducted on the same system. Furthermore, these results are consistent with other established trends. First, in the nerves studied previously, smaller myelinated axons have lower densities of sodium channels than larger diameter axons (see Discussion of reference 44). The axon diameters of the bullfrog olfactory nerve (0.15 μm; see reference 36) are smaller than those of the garfish olfactory (0.24 μm; see reference 7) and the other nonmyelinated nerves (0.6–0.75 μm; see reference 4). Second, the channel density differences parallel differences in the impulse group conduction velocity, which is 0.07–0.075 m/s in the normal bullfrog olfactory nerve (R. Llinas, C. Nicholson, K. Pfenninger, R. Small, and G. Strichartz, unpublished observation), slower than that in the garfish nerve and the other nonmyelinated axons catalogued above (0.1–0.5 m/s; reference 6). Slower conduction velocities—as the lower densities of sodium channels—are associated with axons of smaller average diameter in nonmyelinated fibers.

In growing axons the saturable STX-binding activity, on a fmol/mg wet weight basis, is reduced by about the same fraction whether measured at 4 or 16 nM STX, indicating that the affinity of the receptor is similar to that in the mature nerve and that U_{max} has declined. The full meaning of the reduction in U_{max} can only be understood when the results are corrected for the nerve's axolemmal content. This has necessitated an extensive morphometric analysis of the olfactory nerve. When adjusted for the drastically reduced axolemmal content, the receptor densities reveal an unexpected result: an increase over the values measured in mature axons. Saturable STX binding in the most proximal region of the growing nerves which we could dissect corresponds to a site density of 9.7 per μm^2, in the bone collar region to a density of 8.46 per μm^2, and in the most distal segments to a density of 6.4 per μm^2. These values are 1.3–1.7 times higher than those in the corresponding mature nerve segments. The standard errors of the calculated STX receptor densities in growing nerve are large, ranging from 47 to 74% of the mean values. Variations in the measured U_{max} values for saturable *STX binding to mature nerves and in the relative area determinations together account for only a 12% error; the largest contributor by far is the variation in relative U_{sat} of growing nerve (Table IV), variation that is unavoidable because of the small amount of *STX bound in the saturable mode due to the small mass and reduced axolemmal content of growing nerve and because of the relatively large error in the linear uptake of *STX (for example, see Fig. 3). However, in calculating the standard errors of the receptor site densities we have included every source of variation in the factors and we are confident in the final density values, within a factor of no more than 2. This permits an assignation of STX receptors, and thus, of sodium channels, to a range of IMPs of a large size, as described below.

Correlations with Intramembrane Particles and Other Parameters

Like the changes in STX receptor density, IMP densities are also characterized by gradients in growing nerves (see companion papers, references 35, 36). Is there a size class of IMPs whose density distribution corresponds to that of STX receptors in mature and growing nerves? The STX receptor density of 5.7 per μm^2 in the mature nerve (cf. Fig. 4) falls between those for P-face IMPs of diameter 11.5 to 12.7 nm (12.1/μm^2 and 14/μm^2 in proximal and distal segments, respectively), and 12.8- to 14.0-nm diameter (3–4 μm^2 in both proximal and distal segments).

The spatial density profiles of STX receptors and several IMP size classes in growing nerves are graphed in Fig. 4. The solid lines are quasiexponential curves, describing diffusion equations that fit the observed spatial distribution gradients of different IMP-size classes (35). The comparison of these gradients with that of the STX receptor density indicates that a population of IMPs in the diameter range of 11.5 to 14.0 nm has a density that is spanned by the range of values for STX-binding sites. The density of IMPs of the 10.8-nm-size class in mature nerves is about 35 per μm^2, far in excess of the 5 per μm^2 of STX receptors. IMPs of the next smaller size class, 9.4 nm, occur at much higher densities in both mature (98 and 131 per μm^2 in proximal and distal segments, respectively), and in all segments of growing nerve (124 per μm^2 at the origin and 19 per μm^2 at the most distal terminus). All other size classes of IMPs are also more populous than STX receptors (35).[2] Therefore, based on the comparable densities in both mature and growing nerves, we believe that STX receptors and, thus, sodium channels, may correspond to a group of P-face IMPs in the range of 11.5–14.0-nm diameter.

[2] The nature of E-face IMPs is not clear at present. In olfactory nerve axolemmal they amount to an additional 50%, approximately, for all sizes and regions (41). Even if they had to be added as independent of and equivalent to the respective P-face IMPs, they would not significantly alter the correlation with STX receptors.

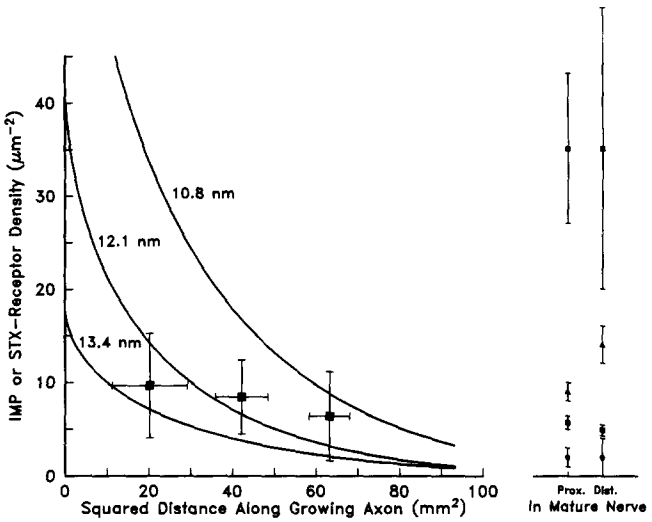

FIGURE 4 The density distribution of STX receptors (■) in growing (*left*) and mature (*right*) nerves compared to that of intramembrane particles (IMPs: curved lines and open symbols). Receptor densities in growing nerves were calculated by multiplying the relative saturable *STX uptake by the absolute axolemmal receptor densities determined for mature nerves (as in Table III). The vertical error bars are the sum of the standard error (expressed as percent of the mean) of the axolemmal area per volume of nerve (cf. Table I) and the standard error of the relative *STX uptake (cf. Table II). Most proximal receptor density was determined from data on intranasal segments and on proximal halves of nerves (intranasal plus bone collar, see Fig. 1). Horizontal error bars show the squares of the standard errors in segmental length determination (six measurements for each). IMP densities of growing axons are shown for three size classes as functions of nerve length according to the moving-boundary diffusion model described in the accompanying paper (35). Measured valued of IMP densities in mature axons are shown on the right (□, 10.8 nm; △, 12.1; ○, 13.4 nm).

Although we cannot exclude the possibility that STX receptors correspond to a subpopulation of a smaller IMP size class, our conclusion is supported by the large size of detergent-solubilized TTX receptors as viewed by high-resolution electron microscopy (8). These receptors appear to be cylinders 4 × 17 nm (width × length). Our findings also support the previously published conclusion, based on morphological and electrophysiological correlations in developing (46) and mature (34) nerves, that IMPs with diameters of ~10 nm and larger are associated with sodium channels in myelinated axons.

The density profiles of STX receptors summarized in Table III and Fig. 4 show that in the most proximal segments of growing axons receptors occur at about twice the density that is measured in mature axons. The gradient of IMPs associated with STX receptors in growing axons may be extrapolated proximally to yield densities at the initial segment of the axon that are 2.5 to 3 times higher than those of mature nerves, where no IMP or STX receptor gradients are detected. (Examination of the perikaryal membranes of growing neurons by freeze-fracture gave the unexpected finding of IMP densities that were comparable to control values. Measurement of STX binding to perikarya buried in the nasal mucosa was not possible.) If functional sodium channels are identified by these particles, then the channel density in the initial segment of growing axons should exceed that of controls. Is there experimental evidence for the physiological consequences of such an increase in sodium channel density? Two examples of the responses of regenerating axons show aspects supportive of our findings. First, in the giant, nonmyelinated motoneuron of the cockroach, axotomy (28) or focal colchicine treatment (27) leads to the appearance of a TTX-sensitive spike invading the perikaryon, where only passive, electrotonically conducted potential changes are normally detected. This is strong evidence for an increase in the excitability and the sodium channel density of the neurite that connects the perikaryon to the neuropil, the normal site of initiation and termination of axonal impulses. The second example concerns changes in the excitability of mammalian motoneurons that appear within 1 wk following axotomy; these include a decrease in the threshhold for impulse initiation (19), the appearance of dendritic "spikes" (18), an increase in the positive overshoot of the intracellular action potential recorded in the perikaryon (23). Such changes are consistent with increases in the sodium channel density at the axon's initial segment (the axon hillock in these cells) and at the dendrites. These electrophysiological results, although measured in axotomized mammalian and insect neurons, are consistent with our observations of changes in STX binding and in the distribution of 11.5–14.0-nm diameter IMPs in growing nonmyelinated axons.

Taken all together, these results suggest that in growing and regenerating axons the density of sodium channels distally is little reduced below that in mature, synapsing fibers, whereas in the neurites most proximal to the perikaryon it is elevated above control levels. Such a situation would arise if the growing or regenerating neuron increased its rate of synthesis and perikaryal insertion of sodium channels, which then diffuse laterally in the plasmalemma, as our model suggests (cf. our companion papers, references 35, 36). As a corollary, this provokes the interesting speculation that the synthesis of sodium channels is modulated (down-regulated) normally by signals carried retrogradely along the axon to the perikaryon. The functional polarity of the plasmalemma in the sprouting neuron, resulting from perikaryal insertion of sodium channels, is further enhanced by the fact that the distal neurite's action potentials appear to be generated mainly by calcium currents, a conclusion supported by electrophysiological evidence (10, 22, 43). The specialized ion conductance properties at the distal tip may be important for mechanisms of directed axonal growth (22, 25) as well as for the function and maintenance of presynaptic structures.

The uneven distribution of STX-binding sites emerges as a general property of growing neurites that is corroborated by the data on IMPs (24, 36) and on glycoconjugates (26). We can conclude, therefore, that the growing axolemma undergoes a maturation process resulting from the insertion of different plasmalemmal components at the growing neuron's opposite poles, the growth cone and the perikaryon. This is followed by mixing of the membrane components by diffusion within the axolemma, as suggested by the freeze-fracture data (see companion papers). Thus, the growing axon provides us with an excellent example of stepwise membrane assembly, combined with gradual functional capacitation in the proximodistal direction.

The authors thank Dr. Richard Ghez for preparing Figure 4, Dr. Rudolpho Llinas fo helpful discussions during the course of this research and Dr. Ann-Judith Silverman for generously permitting the use of her computer facility. The excellent secretarial help of Ms. Anna Malatantis is appreciatively acknowledged.

This research was supported by grants from the U. S. Public Health

Service to G. R. Strichartz (NS18467, NS12828) and to K. H. Pfenniger (NS13466) and from the Muscular Dystrophy Association of America to G. R. Strichartz, and by a fellowship to R. K. Small from the N. Y. State Health Research Council. R. K. Small was a Jordan Fellow of the National Spinal Cord Injury Foundation.

Received for publication 21 September 1982, and in revised form 30 September 1983.

REFERENCES

1. Boyum, A. 1977. Separation of lymphocytes, lymphocyte subgroups, and monocytes: a review. *Lymphology.* 10:71–76.
2. Catterall, W. A. 1975. Cooperation activation of action potential Na^+ ionophore by neurotoxins. *Proc. Natl. Acad. Sci. USA.* 72:1782–1786.
3. Catterall, W. A. 1981. Localization of sodium channels in cultured neural cells. *J. Neurosci.* 1:777–783.
4. Colquhoun, D., R. Henderson, and J. M. Ritchie. 1972. The binding of labelled tetrodotoxin to non-myelinated nerve fibers. *J. Physiol. (Lond.).* 227:95–126.
5. Colquhoun, D., and J. M. Ritchie. 1972. The interaction at equilibrium between tetrodotoxin and mammalian non-myelinated nerve fibers. *J. Physiol. (Lond.).* 221:533–553.
6. Easton, D. M. 1965. Impulses at the artifactual nerve end. *Cold Spring Harbor Symp. Quant. Biol.* 30:15–28.
7. Easton, D. M. 1971. Garfish olfactory nerve: easily accessible source of numerous long, homogeneous, non-myelinated axons. *Science (Wash. DC).* 172:952–955.
8. Ellisman, M. H., W. S. Agnew, J. A. Miller, and S. R. Levinson. 1982. Electronmicroscopic visualization of the tetrodotoxin-binding protein from *Electrophorus electricus. Proc. Natl. Acad. Sci. USA.* 79:4461–4465.
9. Grefrath, S. P., and J. A. Reynolds. 1973. Polypeptide components of an excitable plasma membrane. *J. Biol. Chem.* 248:6091–6094.
10. Grinvald, A., and I. C. Farber. 1981. Optical recording of calcium action potentials from growth cones of cultured neurons with a laser microbeam. *Science (Wash. DC).* 212:1164–1166.
11. Hagiwara, S., and L. Byerly. 1981. Calcium channel. *Annu. Rev. Neurosci.* 4:69–126.
12. Hansen Bay, C. M., and G. R. Strichartz. 1980. Saxitoxin binding to sodium channels of rat skeletal muscles. *J. Physiol. (Lond.).* 300:89–103.
13. Harris, J. B., and M. W. Marshall. 1973. Tetrodotoxin-resistant action potentials in newborn rat muscles. *Nature New Biol.* 243:191–192.
14. Henderson, R., J. M. Ritchie, and G. R. Strichartz. 1973. The binding of labelled saxitoxin to the sodium channels in nerve membranes. *J. Physiol. (Lond.).* 235:783–804.
15. Hille, B. 1970. Ionic channels in nerve membranes. *Prog. Biophys. Mol. Biol.* 21:1–32.
16. Hodgkin, A. L., and A. F. Huxley. 1952. A quantitative description of membrane current and its application to conduction and excitation in nerve. *J. Physiol. (Lond.).* 117:500–544.
17. Krueger, B. K., R. W. Ratzlaff, G. R. Strichartz, and M. P. Blaustein. 1979. Saxitoxin binding to synaptosomes, membranes and solubilized binding sites from rat brain. *J. Membr. Biol.* 50:287–310.
18. Kuno, M., and R. Llinas. 1970. Enhancement of synaptic transmission by dendritic potentials in chromatolysed motoneurones of the cat. *J. Physiol. (Lond.).* 210:807–821.
19. Kuno, M., Y. Miyata, and E. J. Munoz-Martinez. 1974. Differential reaction of fast and slow α-motoneurones to axotomy. *J. Physiol. (Lond.).* 240:725–739.
20. Lawrence, J. C., and W. A. Catterall. 1981. Tetrodotoxin insensitive sodium channels. Ion flux studies of neurotoxin action in a clonal rat muscle cell line. *J. Biol. Chem.* 256:6213–6222.
21. Levinson, S. R. 1975. The purity of tritiated tetrodotoxin as determined by bioassay. *Philos. Trans. R. Soc. (Lond.) B. Biol. Sci.* 270:337–348.
22. Llinas, R., and M. Sugimori. 1979. Calcium conductances in Purkinje cell dendrites: their role in development and integration. *Prog. Brain Res.* 51:323–334.
23. Moolenaar, W. H., and I. Spector. 1978. Ionic currents in cultured mouse neuroblastoma cells under voltage-clamp conditions. *J. Physiol. (Lond.).* 278:265–286.
24. Pfenninger, K. H., and R. P. Bunge. 1974. Freeze-fracturing of nerve growth cones and young fibers: a study of developing plasma membrane. *J. Cell Biol.* 63:180–196.
25. Pfenninger, K. H., and M. P. Johnson. 1982. Nerve growth factor stimulates phospholipid methylation in growing neurites. *Proc. Natl. Acad. Sci. USA.* 78:7797–7800.
26. Pfenninger, K. H., and M. F. Maylie-Pfenninger. 1981. Lectin labeling of sprouting neurons. II. Relative movement and appearance of glycoconjugates during plasmalemmal expansion. *J. Cell Biol.* 89:547–559.
27. Pitman, R. M. 1975. The ionic dependence of action potentials induced by colchicine in an insect motoneurone cell body. *J. Physiol. (Lond.).* 247:511–520.
28. Pitman, R. M., C. D. Tweedle, and M. J. Cohen. 1972. Electrical responses of insect central neurons: augmentation by nerve section or colchicine. *Science (Wash. DC).* 178:507–509.
29. Ritchie, J. M, H. P. Rang, and R. Pellegrino. 1981. Sodium and potassium channels in demyelinated and remyelinated mammalian nerve. *Nature (Lond.)* 294:257–259.
30. Ritchie, J. M., and R. B. Rogart. 1977. The binding of saxitoxin and tetrodotoxin to excitable membranes. *Rev. Physiol. Biochem. Pharmacol.* 79:1–50.
31. Ritchie, J. M., and R. B. Rogart. 1977. Density of sodium channels in mammalian myelinated nerve fibers and nature of the axonal membrane under the myelin sheath. *Proc. Natl. Acad. Sci. USA.* 74:211–215.
32. Ritchie,J. M., and R. B. Rogart. 1977. Characterization of exchange-labelled saxitoxin and the origin of linear uptake by excitable tissue. *Mol. Pharmacol.* 13:1136–1146.
33. Ritchie, J. M., R. B. Rogart, and G. R Strichartz. 1976. A new method for labelling saxitoxin and its binding to non-myelinated fibers of the rabbit vagus, lobster walking leg, and garfish olfactory nerves. *J. Physiol. (Lond.).* 261:477–494.
34. Rosenbluth, J. 1981. Freeze-fracture approaches to ionophore localization in normal and myelin-deficient nerves. *Adv. Neurol.* 31:391–418.
35. Small, R. K., M. Blank, R. Ghez, and K. H. Pfenninger. 1984. Components of the plasma membrane of growing axons: II. Diffusion of membrane protein complexes. 98:1434–1443.
36. Small, R., and K. H. Pfenninger. 198 . Components of the plasma membrane of growing axons: I. Size and distribution of intramembrane particles. 98:1422–1433.
37. Spitzer, N. C. 1979. Ion channels in development. *Annu. Rev. Neurosci.* 2:363–397.
38. Stallcup, W. 1977. Ccomparative pharmacology of voltage-dependent sodium channels. *Brain Res.* 135:37–53.
39. Strichartz, G. R 1982. Structure of the saxitoxin binding site at sodium channels in nerve membranes. Exchange of tritium from bound toxin molecules. *Mol. Pharmacol.* 21:343–350.
40. Strichartz, G. R., D. Bar-Sagi, and J. Prives. 1983. The differential expression of sodium channel activities during the development of chick skeletal muscle cells in culture. *J. Gen. Physiol.* 82:365–384.
41. Strichartz, G. R., and C. M. Hansen Bay. 1981. Saxitoxin binding in nerves from walking legs of the lobster *Homarus Americanus*: two classes of receptors. *J. Gen. Physiol.* 77:205–221.
42. Strichartz, G. R., R. B. Rogart, and J. M. Ritchie. 1979. Binding of radioactivity labelled saxitoxin to the squid giant axon. *J. Membr. Biol.* 48:357–364.
43. Strichartz, G. R., R. Small, C. Nicholson, K. H. Pfenninger, and R. Llinas. 1980. Ionic mechanisms for impulse propagation in growing non-myelinated axons: saxitoxin binding and electrophysiology. *Soc. Neurosci. Abstr.* 6:2252.
44. Tang, C. M., G. R. Strichartz, and R. K. Orkand. 1979. Sodium channels in axons and glial cells of the optic nerve of *Necturus maculosa. J. Gen. Physiol.* 74:629–642.
45. von Muralt, A., E. R. Weiber, and J. V. Howarth. 1976. The optical spike: structure of the olfactory nerve of pike and rapid birefringence changes during excitation. *Pflügers Archiv. Eur. J. Physiol.* 367:67–76.
46. Waxman, S. G., J. A. Black, and R. E. Foster. 1982. Ontogenesis of the axolemma and axo-glial relationships in myelinated fibers: electrophysiological and freeze-fracture correlates of membrane plasticity. *Int. Rev. Neurobiol.* In press.
47. Weibel, E. R., and R. P. Bolender. 1973. Stereological techniques for electron microscopic morphometry. *Principles and Techniques of Electron Microscopy: Biological Applications.* 3:239–291.
48. Weigele, J. B., and R. L. Barchi. 1978. Analysis of saxitoxin binding in isolated rat synaptosomes using a rapid filtration assay. *FEBS (Fed. Eur. Biochem. Soc.) Lett.* 91:310–314.